Acta Cryst. (1998). A**54**, 452–459

A Two-Dimensional Bloch-Wave Method for Dynamical RHEED Calculations

KAZUTO WATANABE,[a]* SHINYA HARA,[b] YOSHIMI HORIO[c] AND IWAO HASHIMOTO[b]

[a]*Tokyo Metropolitan College of Technology, 1-10-40 Higashiohi, Shinagawaku, Tokyo 140, Japan,* [b]*Department of Physics, Science University of Tokyo, 1-3 Kagurazaka, Shinjuku-ku, Tokyo 162, Japan, and* [c]*Daido Institute of Technology 2-21, Daido-cho, Minami-ku, Nagoya 457, Japan. E-mail: shinyahara@aol.com*

(*Received 1 August 1997; accepted 15 January 1998*)

Abstract

A new two-dimensional Bloch-wave method is developed for dynamical reflection high-energy electron diffraction (RHEED) calculations. In this two-dimensional Bloch-wave analysis, the traverse energy and the wave field for each Bloch wave are calculated by a step-by-step R-matrix method. The accuracy of the method is critically examined in comparison with Ichimiya's method on the experimental rocking curve of an Si(001)–2 × 1 surface. It is demonstrated that two-dimensional Bloch-wave analysis can be used to elucidate the mechanism causing the peaks in rocking curves.

1. Introduction

Because of its surface sensitivity, RHEED has become a powerful tool for studies of adsorbed overlayers and reconstructed surfaces. After the discovery of RHEED intensity oscillations by Harris *et al.* (1981), it is well established that the specular-beam intensity for the layer-by-layer growth oscillates with a period corresponding to the deposition of monolayer (Neave *et al.*, 1983; Joyce *et al.*, 1986) or bilayer (Sakamoto *et al.*, 1989; Ohtani *et al.*, 1992; Mitsuishi *et al.*, 1995). Of considerable importance to the development of molecular-beam epitaxy (MBE) has been application of RHEED as *in situ* surface-structure analysis. Recently, an energy-filtered RHEED apparatus (Horio, 1996) has been constructed to determine the more precise surface structure from elastically scattered electrons. In addition, secondary electrons, Auger electrons (Horio & Ichimiya, 1985) and characteristic X-rays (Mitchell *et al.*, 1977) emitted from the surface during RHEED experiments give information on the surface reconstruction or adsorption atoms. As for the analysis, the dynamical calculation must be used for relating the diffraction intensities to the surface structures. Early works of this kind were based on the use of Bethe's n-beam dynamical theory of electron diffraction (Miyake *et al.*, 1954; Collela, 1972) because the Bloch waves offer the site information for a different localization. Hence, this treatment enables diffraction phenomena such as reflection anomalies to be understood in a qualitative sense. In working with this, it is assumed that the crystal potential is a three-dimensional periodic function of the position. Since the period of the crystal potential field ceases at the crystal–vacuum interface plane, it is not completely satisfactory when the surface potential scattering is non-negligible. Furthermore, evanescent waves cannot be taken into account. In principle, a proper method for incorporating the non-periodic variation of the potential in the surface-normal direction is the layer-by-layer method, using two-dimensional periodicity. In fact, most recently published calculations (Maksym & Beeby, 1981; Ichimiya, 1983; Zhao *et al.*, 1988) have been performed by using this method except for Peng & Cowley (1986). The connection between rocking curve and the total wave field are discussed in detail using Bloch-wave and multislice formalisms (Ma & Marks, 1989, 1990, 1991; Wang, 1989). Spence & Kim (1987) considered possible application of resonance scattering to adatom-site determination. However, they do not take advantage of the site information on the localization of each two-dimensional Bloch wave and on their traverse energy like Bethe's eigenvalue method positively, while it has been successful in transmission electron microscopy (TEM) (Fujimoto, 1978; Kambe *et al.*, 1974; Kambe, 1982).

In this paper, the two-dimensional Bloch-wave theory is established in §2 for the dynamical RHEED calculations. The key is to calculate the traverse energy for each two-dimensional Bloch wave, its forward wave and backward wave. Since the rocking curve has only one main peak, an Si(001)–2 × 1 surface is selected to illustrate how the peak arising in a rocking curve is interpreted by the two-dimensional Bloch-wave analysis. The rocking curve is compared with Ichimiya's method on the experimental rocking curve and it is demonstrated that the two-dimensional Bloch-wave analysis is available for elucidation of the origin of the peaks in §3. Finally, a brief summary is given in §4.

2. A generalized two-dimensional Bloch theory

The Schrödinger equation for electrons interacting with a crystal potential is written as

$$E\Psi = [-(\hbar^2/2m)\nabla^2 - eV]\Psi, \quad (1)$$

where E is the energy of incident electrons. The z coordinate is taken parallel to the zone axis. It should be mentioned that for high-energy electrons the relativistic effect is not so far from negligible. For such electrons, the Schrödinger equation with relativistically corrected mass and wavelength is applicable for the straight-forward approximation case (Fujiwara, 1961; Watanabe *et al.*, 1996).

Now, a thick specimen is divided into thin slices, in which a crystal potential is constant in the z direction. In order to obtain information on the traverse energy for each two-dimensional Bloch wave in a slice, the wave function is written by the method of separation of variables,

$$\Psi = b(\boldsymbol{\rho})Z(z), \quad (2)$$

with $\mathbf{r} = (\boldsymbol{\rho}, z)$. Substituting this trial solution (2) into (1) and dividing by $b(\boldsymbol{\rho})Z(z)$ gives

$$\left\{ -\frac{\hbar^2}{2m}\frac{\partial^2}{\partial\rho^2} - (eV + E)\right\} b \Big/ b = \frac{\hbar^2}{2m}\frac{\partial^2 Z}{\partial z^2} \Big/ Z = -\lambda,$$

λ being a constant.

Thus the equation separates into two forms,

$$\left\{ -\frac{\hbar^2}{2m}\frac{\partial^2}{\partial\rho^2} - (eV + E)\right\} b = -\lambda b \quad (3)$$

and

$$\frac{\hbar^2}{2m}\frac{\partial^2 Z}{\partial z^2} = -\lambda Z. \quad (4)$$

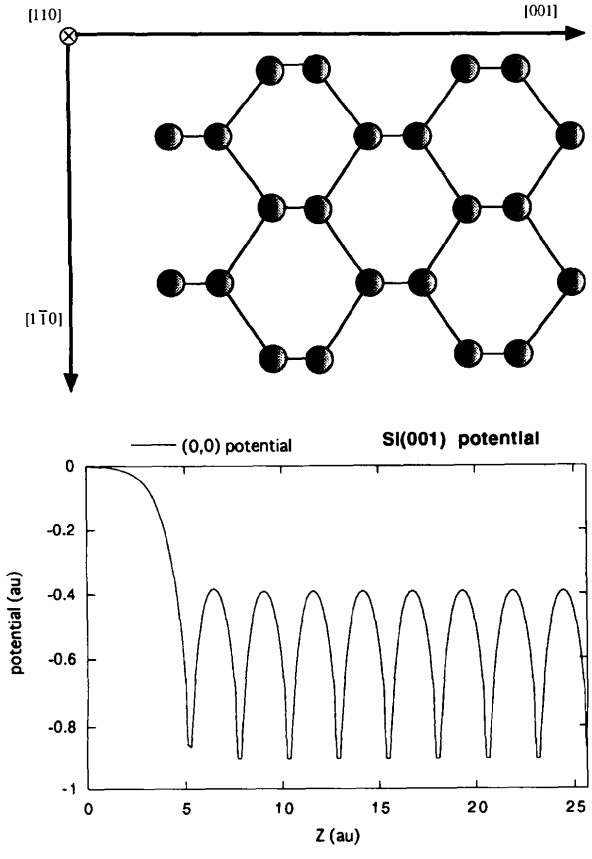

Fig. 1. A side view of the (110) plane and the real part of the potential component V_{00}.

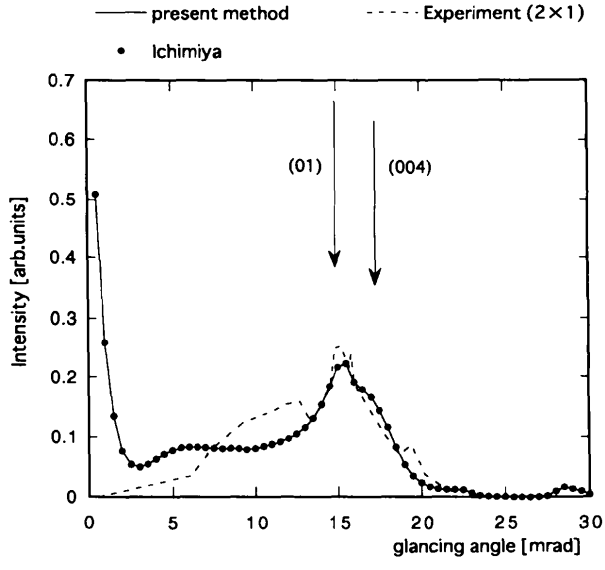

Fig. 2. Rocking curves of 00 rod beam at [110] incidence of Si(001)–2 × 1. Dashed line: experimental data, solid line: calculated with the present method. Circles: calculated with Ichimiya's method. The arrows denote the position of the (004) primary Bragg condition and the (01) vacuum threshold condition.

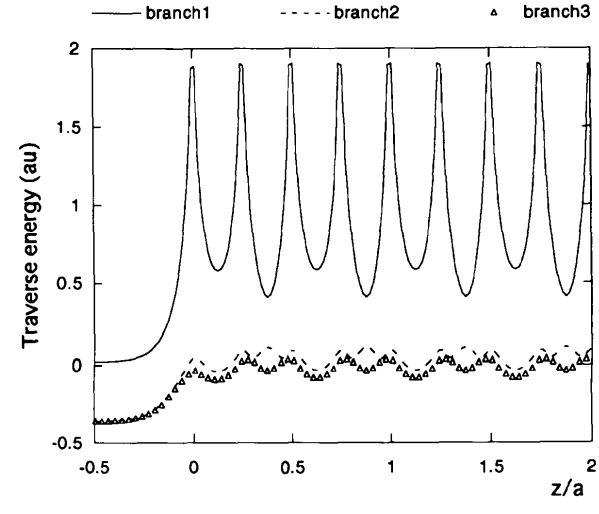

Fig. 3. Traverse energies for each Bloch wave at a glancing angle of 3.5 mrad.

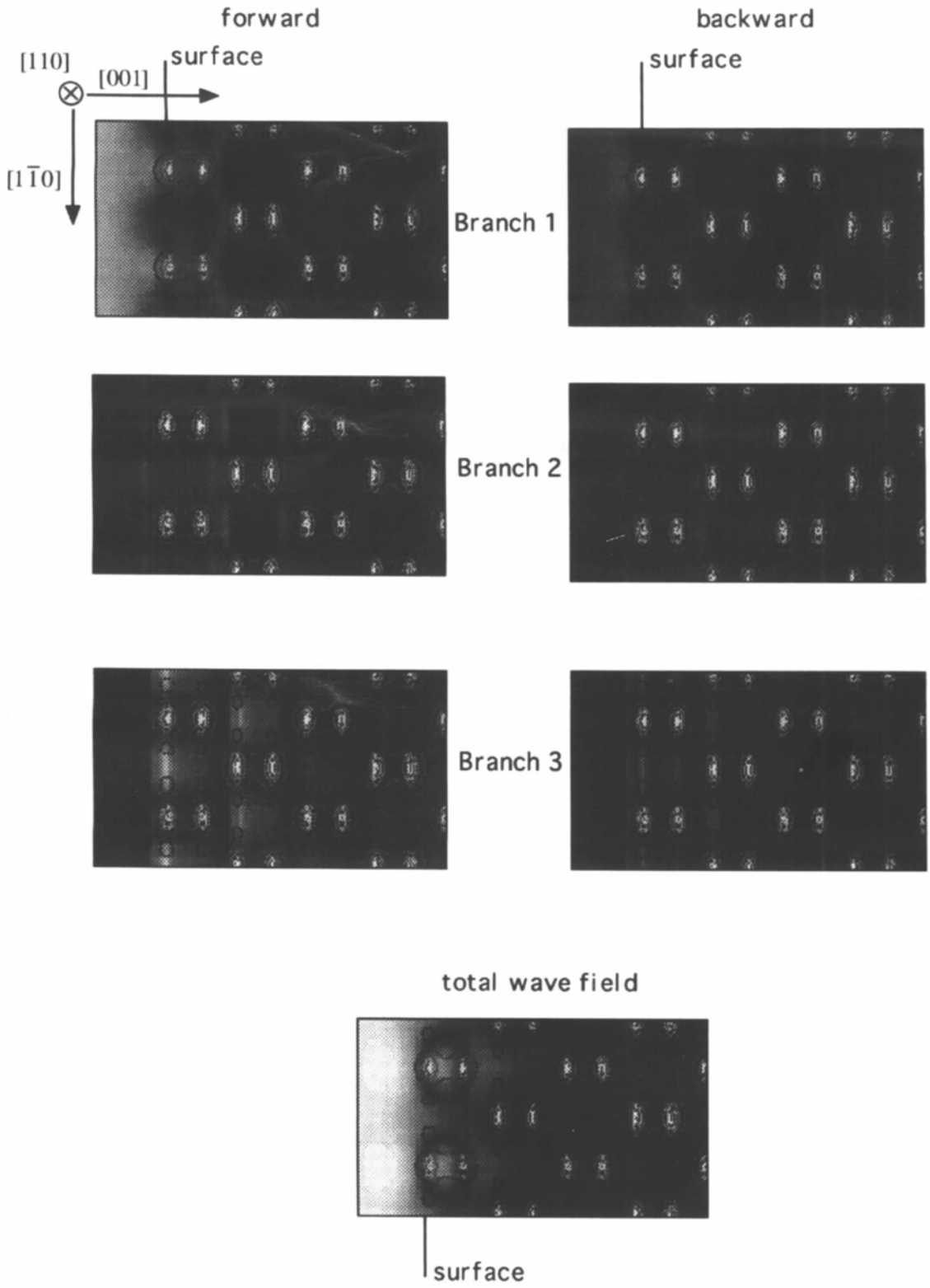

Fig. 4. Wave fields for each Bloch wave and the total wave field at 3.5 mrad.

Using the two-dimensional Fourier expansion of $b(\boldsymbol{\rho})$, the differential equation (3) at the ith slice is transformed into the jth set of eigenvalue equations for $C^i_{\mathbf{g}_\parallel,j}(z)$ and λ^i_j:

$$(\hbar^2/2m)(\mathbf{k}_\parallel+\mathbf{g}_\parallel)^2 C^i_{\mathbf{g}_\parallel,j} - e\sum V_{\mathbf{g}_\parallel-\mathbf{g}'_\parallel} C^i_{\mathbf{g}'_\parallel,j} = (E-\lambda^i_j)C^i_{\mathbf{g}_\parallel,j}, \tag{5}$$

where $\mathbf{k}=(\mathbf{k}_\parallel, k_z)$ and $\mathbf{g}_\parallel$ are the incident wave vector and the two-dimensional reciprocal-lattice vectors, respectively, and

$$V(\mathbf{r}) = \sum_{\mathbf{g}_\parallel} V_{\mathbf{g}_\parallel}(z)\exp\{i(\mathbf{g}_\parallel\cdot\boldsymbol{\rho})\},$$

with $V_{\mathbf{g}_\parallel}(z) = V^i_{\mathbf{g}_\parallel}$ in the ith slice.

In matrix form,

$$\boldsymbol{Q}^i\cdot\boldsymbol{C}^i_j = \lambda^i_j\boldsymbol{C}^i_j. \tag{6}$$

The eigenvalue λ^i_j, referred to as the traverse energy, and the associated eigenvectors $\boldsymbol{C}^i_{\mathbf{g}_\parallel,j}$ can be obtained by solving the eigensystem (6). The two-dimensional Bloch waves are given by these eigenvectors and eigenvalues. A similar treatment can be seen in an earlier work for the TEM case, where the eigenvalue of $E-\lambda$ corresponds to the 'transverse' energy parallel to the surface (Kambe *et al.*, 1974). For a given eigenvalue λ^i_j, equation (4) can be analytically solved. Thus, the total wave function at the ith slice can be written as

$$\begin{aligned}\Psi_i(\boldsymbol{\rho},z) = &\sum_j \alpha^i_j \sum_{\mathbf{g}_\parallel} C^i_{\mathbf{g}_\parallel,j}\exp[i(2m\lambda^i_j/\hbar^2)^{1/2}z]\\ &\times\exp[i(\mathbf{k}_\parallel+\mathbf{g}_\parallel)\cdot\boldsymbol{\rho}]\\ &+\sum_j \beta^i_j\sum_{\mathbf{g}_\parallel} C^i_{\mathbf{g}_\parallel,j}\exp[-i(2m\lambda^i_j/\hbar^2)^{1/2}z]\\ &\times\exp[i(\mathbf{k}_\parallel+\mathbf{g}_\parallel)\cdot\boldsymbol{\rho}],\end{aligned} \tag{7}$$

where $(2m\lambda^i_j/\hbar^2)^{1/2} = \zeta^i + i\eta^i$. The excitation amplitudes α^i_j and β^i_j can be determined from the boundary conditions. In the matrix notation, the column vector $\boldsymbol{\Phi}_i$ composed of the wave function and its derivative is given by

$$\begin{aligned}\boldsymbol{\Phi}_i(z) &= \begin{bmatrix}\{\Phi^{\mathbf{g}_\parallel}_i\}\\ \{\Phi'^{\mathbf{g}_\parallel}_i\}\end{bmatrix}\\ &= \begin{bmatrix}\{C^i_{\mathbf{g}_\parallel,j}\} & \{C^i_{\mathbf{g}_\parallel,j}\}\\ \{i(2m\lambda^i_j/\hbar^2)^{1/2}C^i_{\mathbf{g}_\parallel,j}\} & \{-i(2m\lambda^i_j/\hbar^2)^{1/2}C^i_{\mathbf{g}_\parallel,j}\}\end{bmatrix}\\ &\quad\times\begin{bmatrix}\gamma_i(z) & 0\\ 0 & \gamma'_i(z)\end{bmatrix}\begin{bmatrix}(\alpha_i)\\ (\beta_i)\end{bmatrix}\\ &= \boldsymbol{C}_i\cdot\boldsymbol{\Gamma}_i(z)\begin{bmatrix}(\alpha_i)\\ (\beta_i)\end{bmatrix},\end{aligned} \tag{8}$$

where γ_i and γ'_i are diagonal matrices with $\gamma_{im,m} = \exp[i(2m\lambda^i_m/\hbar^2)^{1/2}z]$ and $\gamma'_{im,m} = \exp[-i(2m\lambda^i_m/\hbar^2)^{1/2}z]$, respectively. The result is similar to the general dynamical theory (Peng & Whelan, 1990*a*,*b*; Peng *et al.*, 1996*a*,*b*,*c*). The column vectors Φ_i at the top and bottom of the ith slice are connected with the so-called transfer matrix $\boldsymbol{M}_i$ ($2N\times 2N$) as

$$\begin{aligned}\Phi_i(z^t_i) &= \boldsymbol{C}_i\cdot\boldsymbol{\Gamma}_i(z^t_i)\{\boldsymbol{C}_i\cdot\boldsymbol{\Gamma}_i(z^b_i)\}^{-1}\Phi_i(z^b_i)\\ &= \boldsymbol{C}_i\cdot\boldsymbol{\Gamma}_i(z^t_i - z^b_i)\cdot(\boldsymbol{C}_i)^{-1}\cdot\boldsymbol{\Phi}_i(z^b_i)\\ &= \boldsymbol{M}_i\cdot\boldsymbol{\Phi}_i(z^b_i).\end{aligned} \tag{9}$$

This matrix representation is formally equivalent to those in other RHEED methods but differs in the treatment of the relevant matrices. For a thick slab composed of an assembly of thin slices, equation (9) is generalized to give

$$\boldsymbol{\Phi}_1(z^t_1) = \boldsymbol{M}_1\boldsymbol{\Phi}_1(z^b_1) = \prod_i \boldsymbol{M}_i\boldsymbol{\Phi}_n(z^b_n) = \boldsymbol{M}\boldsymbol{\Phi}_n(z^b_n), \tag{10}$$

with

$$\boldsymbol{M} = \prod_i\begin{bmatrix}q^i_{11} & q^i_{12}\\ q^i_{21} & q^i_{22}\end{bmatrix}.$$

At the slab top ($z=0$), $\boldsymbol{\Phi}_0$ including the incident and reflected waves is given by

$$\boldsymbol{\Phi}_0 = \begin{pmatrix}\{(\varphi\delta_{\mathbf{g}_\parallel,0} + r_{\mathbf{g}_\parallel})\}\\ \{i(k_{g_\perp}\varphi\delta_{\mathbf{g}_\parallel,0} - k_{g_\perp}r_{\mathbf{g}_\parallel})\}\end{pmatrix}, \tag{11}$$

where $k^2_{g_\perp} = (2m/\hbar^2)E - (\mathbf{k}_\parallel+\mathbf{g}_\parallel)^2$ and $r_{\mathbf{g}_\parallel}$ are the reflection coefficients. $\boldsymbol{\Phi}_b$ at the slab bottom ($z=z_b$) has the form

$$\boldsymbol{\Phi}_b = \begin{pmatrix}\{t_{\mathbf{g}_\parallel}\exp(ik_{g_\perp}\cdot z_b)\}\\ \{ik_{g_\perp}t_{g_\parallel}\exp(ik_{g_\perp}\cdot z_b)\}\end{pmatrix}, \tag{12}$$

with the transmission coefficients $t_{\mathbf{g}_\parallel}$. Hence, substituting equations (11) and (12) into (10),

$$\boldsymbol{\Phi}_0 = \boldsymbol{M}\cdot\boldsymbol{\Phi}_b. \tag{13}$$

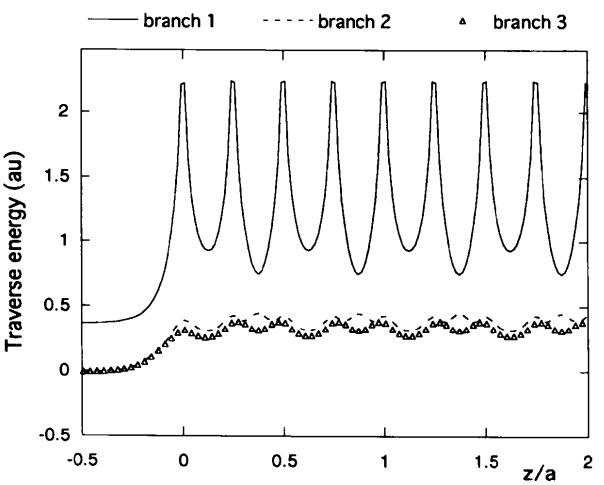

Fig. 5. Traverse energies for each Bloch wave at 15 mrad.

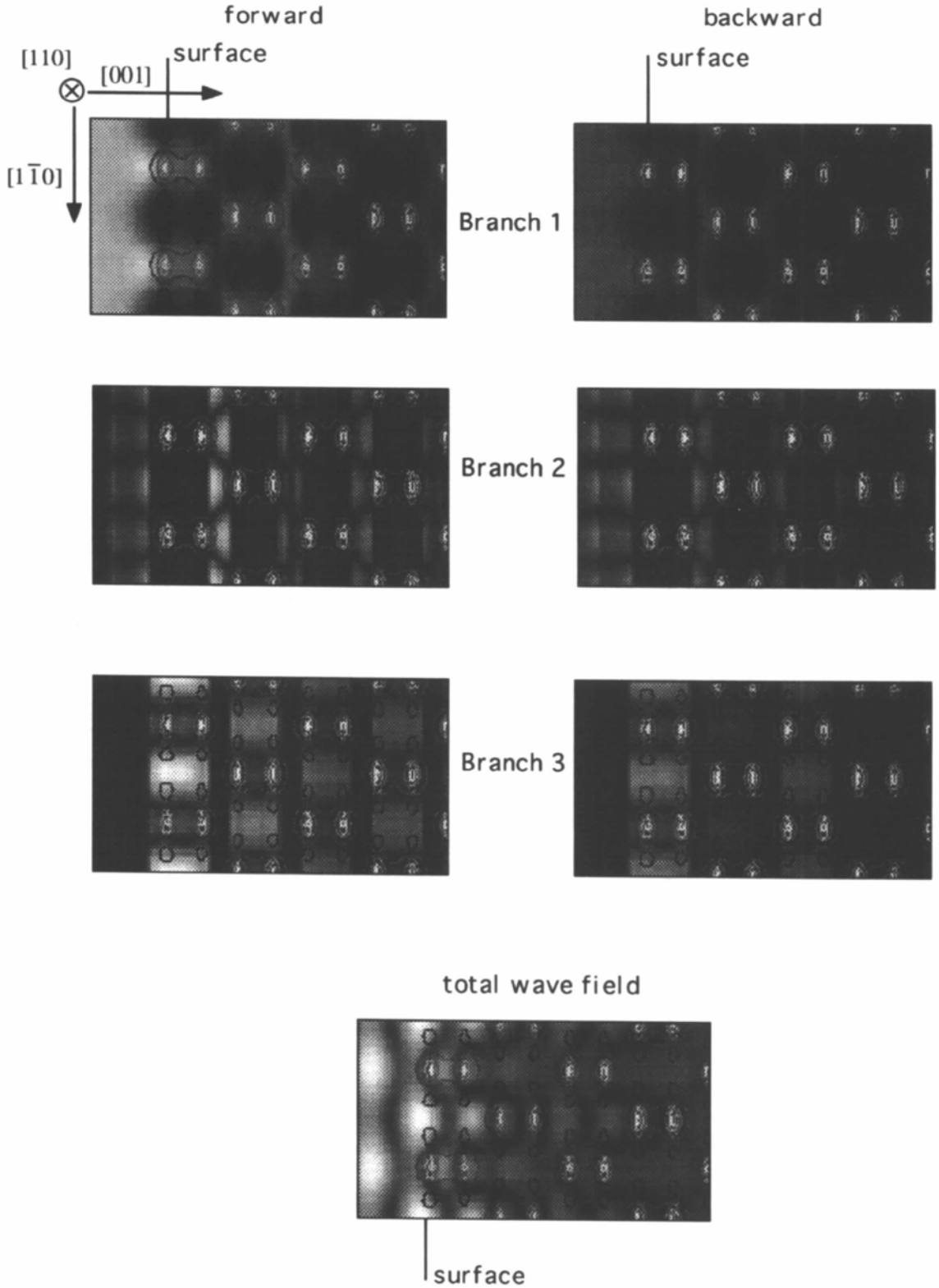

Fig. 6. Wave fields for each Bloch wave and the total wave field at 15 mrad.

When the scattering matrix includes evanescent waves, the $\boldsymbol{M}$ matrix diverges quickly. In order to avoid this divergence, the R-matrix scheme (Light & Walker, 1976) has been introduced. The R matrix $\boldsymbol{R}_i$ is defined here so as to relate the $\boldsymbol{\Phi}_i(z)$ vector and $\boldsymbol{\Phi}_i'(z)$ at the ith slice, so that

$$\boldsymbol{\Phi}_i'(z_i^t) = \boldsymbol{R}_i \cdot \boldsymbol{\Phi}_i(z_i^t). \tag{14}$$

From the boundary condition at the bottom [equation (12)], $\boldsymbol{R}_n$ is given by

$$\boldsymbol{R}_n = (i\boldsymbol{K} \cdot \boldsymbol{q}_{12}^n - \boldsymbol{q}_{22}^n)^{-1} \cdot (\boldsymbol{q}_{21}^n - i\boldsymbol{K} \cdot \boldsymbol{q}_{11}^n) \tag{15}$$

with the diagonal matrix $K_{ii} = k_{g_\perp}$. The following recursion relation for the R matrix $\boldsymbol{R}_i$ is derived from (8) and (9):

$$\begin{aligned}\boldsymbol{R}_i = &\{(\boldsymbol{q}_{21}^{i+1} + \boldsymbol{q}_{22}^{i+1} \cdot \boldsymbol{R}_{i+1})^{-1} \cdot \boldsymbol{q}_{22}^i \\ &- (\boldsymbol{q}_{11}^{i+1} + \boldsymbol{q}_{12}^{i+1} \cdot \boldsymbol{R}_{i+1})^{-1} \cdot \boldsymbol{q}_{12}^i\}^{-1} \\ &\cdot \{(\boldsymbol{q}_{11}^{i+1} + \boldsymbol{q}_{12}^{i+1} \cdot \boldsymbol{R}_{i+1})^{-1} \cdot \boldsymbol{q}_{11}^i \\ &- (\boldsymbol{q}_{21}^{i+1} + \boldsymbol{q}_{22}^{i+1} \cdot \boldsymbol{R}_{i+1})^{-1} \cdot \boldsymbol{q}_{21}^i\}.\end{aligned} \tag{16}$$

At the top, the reflection vector $\mathbf{r}$ is given from (11) by the incident wavevector $(\varphi\delta_{\mathbf{g}_\parallel,0})$,

$$\begin{aligned}\mathbf{r} = &\{(\boldsymbol{q}_{11}^1 + \boldsymbol{q}_{12}^1 \cdot \boldsymbol{R}_1)^{-1} + i(\boldsymbol{q}_{21}^1 + \boldsymbol{q}_{22}^1 \cdot \boldsymbol{R}_1)^{-1} \cdot \boldsymbol{K}\}^{-1} \\ &\cdot \{i(\boldsymbol{q}_{21}^1 + \boldsymbol{q}_{22}^1 \cdot \boldsymbol{R}_1)^{-1} \cdot \boldsymbol{K} \\ &- (\boldsymbol{q}_{11}^1 + \boldsymbol{q}_{12}^1 \cdot \boldsymbol{R}_1)^{-1}\} \cdot (\varphi\delta_{\mathbf{g}_\parallel,0}).\end{aligned} \tag{17}$$

Now, to calculate wave fields at each slice, excitation amplitudes, *i.e.* $\boldsymbol{\alpha}_i$ and $\boldsymbol{\beta}_i$, are evaluated using the same $\boldsymbol{R}_i$ matrix successively, starting from the top to the bottom by using equations (8), (11), (14), (15), (16) and (17).

3. Results and discussion

To give a qualitative description, the calculations were made in a simple way, where the surface reconstruction was not considered and only three beams, 00, 01 and $0\bar{1}$ rods, were taken into account. The accelerating voltage and the azimuthal angle were fixed at 40 kV and in the [110] direction in order to create the same condition as the experiment (Sakamoto *et al.*, 1987). The reflectivity can be given as the perpendicular component of the reflected flux relative to the perpendicular component of the incident flux. Fig. 1 shows a side view of a (110) plane and the real part of the potential component V_{00}. The surface region was made up of four layers having depth $a/4$ (a is the lattice constant) and the substrate of 40 layers. Using this structure, a real potential $V_{\mathbf{g}_\parallel}(z)$ was calculated by a Fourier expansion of the electron scattering factors tabulated by Doyle & Turner (1968). Inelastic scattering was included as an imaginary potential taken as 10% of the real one and every slice thickness was set at $a/120$.

The rocking curves calculated by the present method and Ichimiya's method are shown in Fig. 2 together with the experimental result. The measured peak does not correspond to the primary Bragg condition but agrees with the vacuum threshold one. Comparison of the experimental and the theoretical results shows that the main peak is reproduced well even with the simple three-beam calculations, while there is little deviation in the glancing angle. The excellent agreement of the two theoretical results leads to the fact that the present method is on a level with Ichimiya's method in accuracy. The real part of the traverse energy for each Bloch wave and its forward, backward and total wave fields are shown for three glancing angles in Figs. 3–8, where the contour maps display the potential-energy profile on a (110) plane. The term 'wave field' means the spatial intensity distribution formed by the incident electrons. The wave fields are mapped by gray scale and normalized at the maximum value. It is well known in transmission electron microscopy that a traverse energy or a wave vector whose Bloch wave mainly concentrates on the atomic sites is on average larger than that located on the tunneling sites because the traverse energy increases through potential energy while the total energy of each Bloch wave is a constant and equal to an incident electron energy for elastic scattering. Fig. 3 shows that only one Bloch wave at 3.5 mrad (branch 1) can be transmitted into the crystal but branches 2 and 3 are evanescent having negative traverse energy above the top surface of the crystal. In Fig. 4, the forward and backward wave fields for branch 1 concentrate on the atomic sites, thus largely decaying away from the surface. The forward and backward wave fields for branches 2 and 3 are located on the tunneling sites. The total wave field is mainly contributed by the wave fields of branch 1. As shown in Fig. 5, the real parts of traverse energies for branches 2 and 3 become

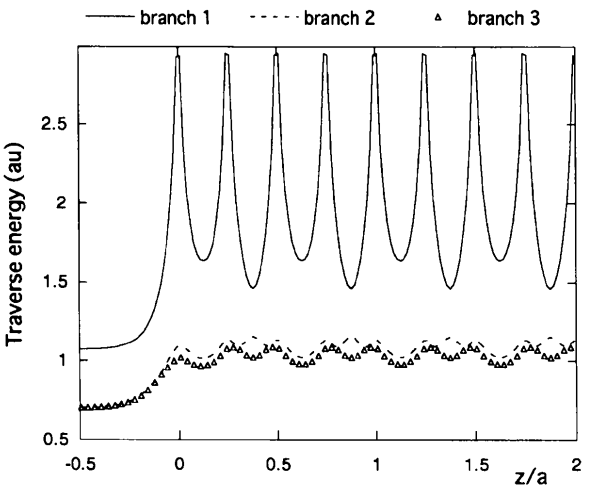

Fig. 7. Traverse energies for each Bloch wave at 26.5 mrad.

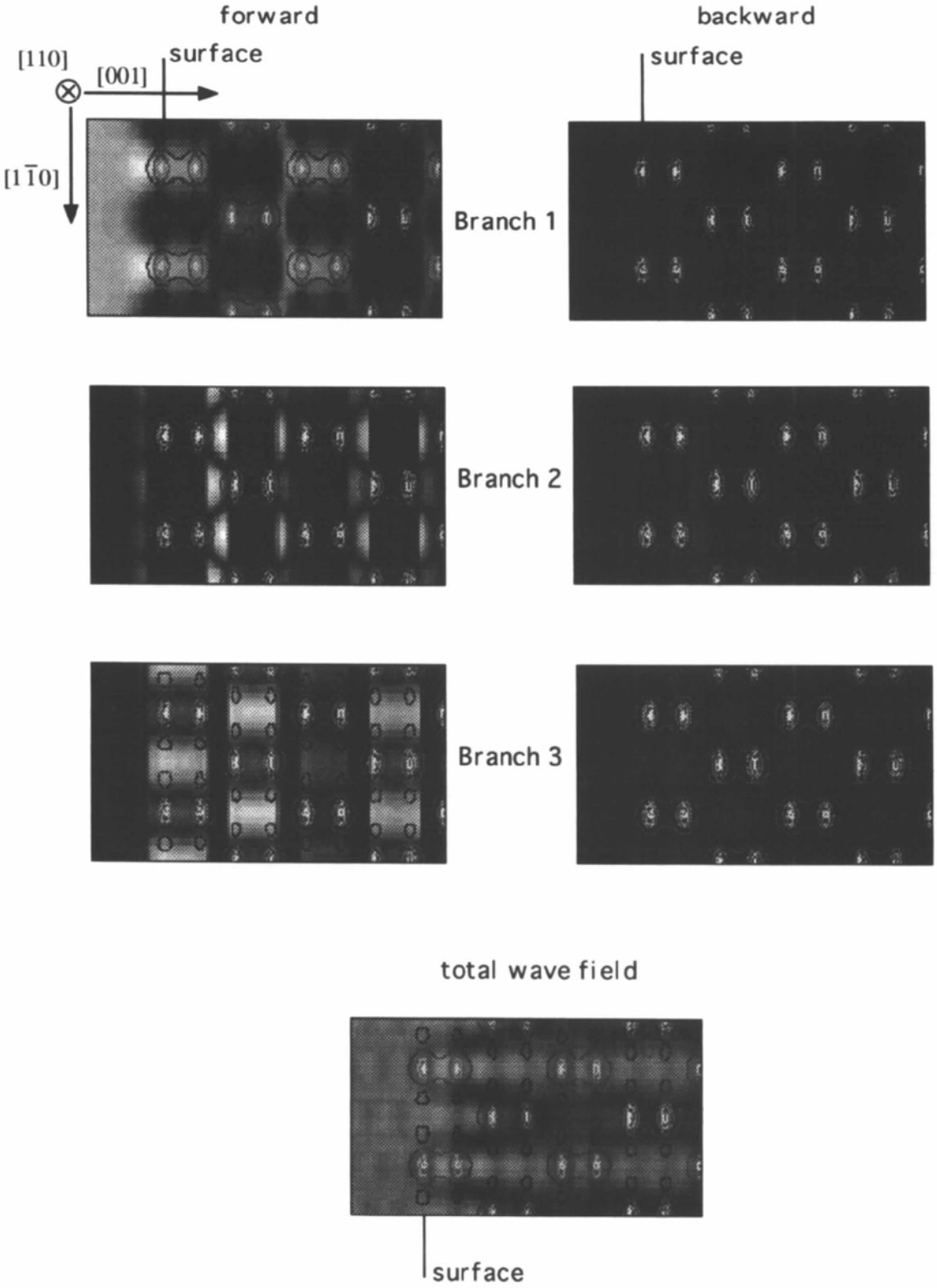

Fig. 8. Wave fields for each Bloch wave and the total wave field at 26.5 mrad.

positive just above the top of the crystal surface at the peak angle (15 mrad) and vary with thickness inside the crystal. This fact gives rise to the refraction variations, so that multilayers are stacked with small refraction layers and large refraction layers in turn. It is accordingly expected that the localization of Bloch waves occurs in the first several atomic layers parallel to the surface. In fact, the localization of backward Bloch waves for branch 2 arises mainly above the top surface and that for branch 3 on the tunneling site at the first and second layers (Fig. 6). The concept of the localization has been introduced as a threshold condition (Maksym & Beeby, 1982; Marten & Meyer-Ehmsen, 1985; Peng *et al.*, 1996*b*,*c*) and the localization on the tunneling sites at the peak position has been demonstrated in the work of Horio & Ichimiya (1996) who made calculations for an Si(111) surface. The peak in the rocking curve cannot be identified as the primary Bragg peak because the periodicity of the wave fields associated with the 004 Bragg peak is not shown. It is also worth noting that such discussions cannot be made by just the difference in total wave field. The real parts of the traverse energies and the wave fields associated with 26.5 mrad are also displayed in Figs. 7 and 8. The three kinds of positive traverse energies increase with the glancing angle, so that the forward wave field for each Bloch wave penetrates into a deeper region and the intensity of the backward wave field is too weak to cause the localization of the wave fields.

4. Summary

A two-dimensional Bloch-wave method is developed for dynamical RHEED calculation. The present method brings about the same level of the accuracy as Ichimiya's method in rocking-curve calculations. The two-dimensional Bloch-wave analysis has been introduced to clarify the nature of peaks arising in rocking curves. The key to a threshold peak is the emergence of a Bloch wave above the top surface of the crystal which does not have sufficient energy to escape into the deeper region and is channeled through the topmost layers parallel to the surface. The present interpretation may have general validity for the complex rocking curve having many peaks. Of course, our present calculations are insufficient to make a quantitative comparison with RHEED experiment. Further studies are necessary to clarify the contributions of surface reconstruction under convergent calculations.

We appreciate valuable discussions with and useful comments from Dr K. Kambe.

References

Collela, R. (1972). *Acta Cryst.* A**28**, 11–15.
Doyle, P. A. & Turner, P. S. (1968). *Acta Cryst.* A**24**, 390–397.
Fujimoto, F. (1978). *Phys. Status Solidi A*, **5**, 99–106.
Fujiwara, K. (1961). *J. Phys. Soc. Jpn*, **14**, 2226–2238.
Harris, J., Joyce, B. & Dobson, P. J. (1981). *Surf. Sci.* **103**, L90–L96.
Horio, Y. (1996). *Jpn. J. Appl. Phys.* **35**, 3559–3564.
Horio, Y. & Ichimiya, A. (1985). *Surf. Sci.* **164**, 589–601.
Horio, Y. & Ichimiya, A. (1996). *Surf. Sci.* **348**, 344–358.
Ichimiya, A. (1983). *Jpn. J. Appl. Phys.* **22**, 176–180.
Joyce, B. A., Dobson, P. J., Neave, J. H., Woodbridge, J., Zhang, J., Larsen, P. K. & Bogel, G. (1986). *Surf. Sci.* **168**, 423–438.
Kambe, K. (1982). *Ultramicroscopy*, **10**, 223–228.
Kambe, K., Lehmpfuhl, G. & Fujimoto, F. (1974). *Z. Naturforsch. Teil A*, **29**, 1034–1044.
Light, J. C. & Walker, R. B. (1976). *J. Chem. Phys.* **65**, 4272–4282.
Ma, Y. & Marks, L. D. (1989). *Acta Cryst.* A**45**, 174–182.
Ma, Y. & Marks, L. D. (1990). *Acta Cryst.* A**46**, 11–32.
Ma, Y. & Marks, L. D. (1991). *Acta Cryst.* A**47**, 707–715.
Maksym, P. A. & Beeby, J. L. (1981). *Surf. Sci.* **110**, 423–438.
Maksym, P. A. & Beeby, J. L. (1982). *Appl. Surf. Sci.* **11/12**, 663–676.
Marten, H. & Meyer-Ehmsen, G. (1985). *Surf. Sci.* **151**, 570–584.
Mitchell, D. F., Swell, S. B. & Cohen, M. (1977). *Surf. Sci.* **69**, 310–324.
Mitsuishi, K., Hashimoto, I., Sakamoto, K., Sakamoto, T. & Watanabe, K. (1995). *Phys. Rev. B*, **15**, 10748–10751.
Miyake, S., Kohra, K. & Takagi, M. (1954). *Acta Cryst.* **7**, 393–401.
Neave, J. H., Joyce, B. A., Dobson, P. J. & Norton, N. (1983). *Appl. Phys.* A**31**, 1–8.
Ohtani, N., Molker, S. M., Zhang, J. & Joyce, B. A. (1992). *Appl. Phys. Lett.* **61**, 1399–1401.
Peng, L.-M. & Cowley, J. M. (1986). *Acta Cryst.* A**42**, 545–552.
Peng, L.-M., Dudarev, S. L. & Whelan, M. J. (1996*a*). *Acta Cryst.* A**52**, 471–475.
Peng, L.-M., Dudarev, S. L. & Whelan, M. J. (1996*b*). *Acta Cryst.* A**52**, 909–922.
Peng, L.-M., Dudarev, S. L. & Whelan, M. J. (1996*c*). *Surf. Sci.* **351**, L245–L252.
Peng, L.-M. & Whelan, M. J. (1990*a*). *Proc. R. Soc. London Ser. A*, **431**, 111–124.
Peng, L.-M. & Whelan, M. J. (1990*b*). *Proc. R. Soc. London Ser. A*, **431**, 125–142.
Sakamoto, T., Kawai, N., Nakagawa, T., Ohta, K. & Kojima, T. (1989). *Appl. Phys. Lett.* **47**, 617–619.
Sakamoto, T., Sakamoto, K., Nagao, S., Hashiguchi, G., Kuniyoshi, K. & Bando, Y. (1987). *Thin Film Growth Techniques for Low-Dimensional Structures*, edited by R. F. C. Farrow, S. S. P. Parkin, P. J. Dobson, J. H. Neave & A. S. Arrott, pp. 225–236. New York: Plenum Press.
Spence, J. C. H. & Kim, Y. (1987). *Reflection High-Energy Electron Diffraction and Reflection Electron Imaging of Surfaces*, edited by P. K. Larsen & P. J. Dobson, pp. 117–129. New York: Plenum Press.
Wang, Z. L. (1989). *Philos. Mag.* B**60**, 205–222.
Watanabe, K., Hara, S. & Hashimoto, I. (1996). *Acta Cryst.* A**52**, 379–384.
Zhao, T. C., Poon, H.C. & Tong, S. Y. (1988). *Phys. Rev. B*, **38**, 1172–1182.